DOI: 10.1002/anie.201208793

Electrochemistry

Anodic Formation of Self-Organized Cobalt Oxide Nanoporous Layers**

*Chong-Yong Lee, Kiyoung Lee, and Patrik Schmuki**

Cobalt oxide materials have shown great potential for applications such as magnetic data storage devices, heterogeneous catalysts, lithium-ion battery materials, supercapacitors and solid-state sensors.[1,2] Most recently, cobalt-based nanostructures have also attracted wide interest as a catalyst for water oxidation and a cheap and abundant alternative to ruthenium and iridium-based materials. Particularly, the work of Nocera and co-workers on the in situ formation of a cobalt-based material through electrodeposition has stimulated considerable research activities in the field of water oxidation catalysis.[3] Typically, the approaches to synthesizing defined compound oxides or other nanostructures such as nanoporous, nanotubular, nanorod, and nanowire morphologies are either template-based, for example, through porous anodic alumina,[4] SBA,[5] viruses,[6] or template-free hydro- and solvothermal[7] techniques.

One of the most elegant and attractive approaches to form nanostructures of metal oxides is through self-organizing electrochemical anodization. The prototype of this process is the growth of highly ordered porous alumina structures which had been achieved by Masuda and Fukuda in 1995 by establishing an optimized oxide formation/dissolution equilibrium during anodization of aluminium in an acidic solution.[8] In 1999, Zwilling et al.[9] demonstrated that self-organized TiO_2 nanopores or nanotubes can be obtained through anodization of Ti metal sheets in a fluoride-containing electrolyte. This simple and low-cost fluoride-based approach to form nanoporous layers has then been extended to oxide nanotube or nanopore formation of numerous other metals such as Ta, Hf, W, Zr, Nb, Fe, and V, as well as many alloys.[10,11] The key role of addition of fluorides is to establish sufficient solubility of the oxide [by formation of MF_x^{n-} complexes] to allow for a sufficient dissolution rate during anodization, to establish optimized self-organizing conditions.[12]

Nevertheless, up to now, there is no report on the successful anodization of cobalt to obtain self-ordered nanostructured oxide layers. The main difficulty in anodizing cobalt is intrinsically connected with one of its most promising practical applications, that is that cobalt oxides are highly electrocatalytically active towards water oxidation. In other words, when an anodic voltage is applied in an aqueous electrolyte, the preferred reaction is the oxidation of the water at a comparably low potential as illustrated in Figure 1 a. This prevents the application of higher anodization voltages (typically some 10 V) from growing a high-field oxide and from establishing self-organization conditions. Herein, we show how to overcome the problem by combining a number of strategies to retard the reaction rate of water oxidation and favor oxide formation. This enables the successful anodic growth of high-aspect-ratio ordered nanoporous layers on a cobalt foil as shown in Figure 1. These structures can be grown up to several 10 micrometers long with an ordered pore arrangement and diameters in the range of 50 to 100 nm.

The key parameters to slow down the oxygen evolution kinetics (and favor oxide growth) are an electrolyte with a low but optimized water content and anodization at reduced temperature. Additionally, an optimized oxide dissolution rate through adjusting the fluoride ion content and pH is needed to allow for self-organization. In this context it is noteworthy to mention that the pH not only influences the dissolution kinetics of the oxide (in the interplay with fluorides) but also strongly affects the oxygen evolution kinetics, which is in line with a recent report by Gerken et. al[13] indicating a strong pH dependence of the mechanism of electrolysis of Co_{aq}^{II} in buffered HF/F^- electrolytes. Following these principles, a step-by-step optimization of anodization parameters (as outlined in Table S1 and Figures S1–S8 in the Supporting Information) enabled the formation of porous cobalt oxide structures and led to a progressively improved degree of self-organization of the resulting morphologies.

Figure 1 b,c shows top and side view SEM images of the nanoporous layers formed on a cobalt foil after anodization in a mixed ethylene glycol and glycerol solvent (volume ratio of 1 to 3) containing 3 M H_2O and 0.54 M NH_4F at 50 V at 0 °C for 16 h. Depending on the anodization time, the thickness of the ordered structure can be adjusted from some hundred nanometers to several micrometers (Figure 1 e). In every case a comparably smooth surface is achievable (Figure 1 d). The porous layer exhibits the typical scalloped bottom view morphology of self-ordered anodized metal oxides (see Figure S1 c). Additional morphological details are shown in Figure S1.

The parameter range for successful self-organization is, in comparison to other self-organizing systems, comparably narrow.[10f] This is illustrated with some examples in Figure 2. A very good indication for a successful growth of

[*] Dr. C.-Y. Lee, K. Lee, Prof. Dr. P. Schmuki
Department of Materials Science and Engineering
University of Erlangen-Nuremberg
Martensstrasse 7, 91058 Erlangen (Germany)
E-mail: schmuki@ww.uni-erlangen.de

[**] We acknowledge the financial support from the DFG and the DFG cluster of excellence (EAM). Helga Hildebrand and Dr. Matthias Moll are acknowledged for the X-ray photoelectron spectroscopy and oxygen measurements, respectively.

Supporting information for this article is available on the WWW under http://dx.doi.org/10.1002/anie.201208793.

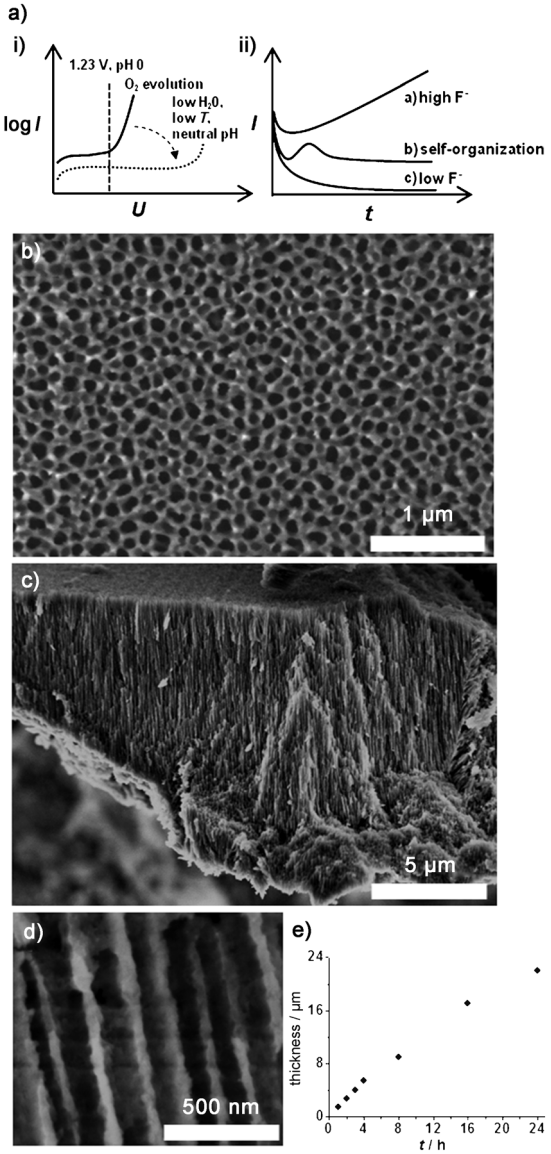

Figure 1. Schematic illustration for a) current–voltage and current–time curves that illustrate the essential parameters to suppress oxygen evolution, to establish and favor a self-organizing anodic porous oxide formation. Top (b) and side (c, d) views of SEM images of the nanoporous anodic layer grown under optimized anodization conditions (a mixed glycerol and ethylene glycol solution with a volume ratio of 3 to 1 containing 3 M H_2O and 0.54 M NH_4F, anodization at 50 V, 0 °C for 16 h). d) Regular channels at the nanoporous layer. e) Thickness evolution with time under the conditions as described in (d).

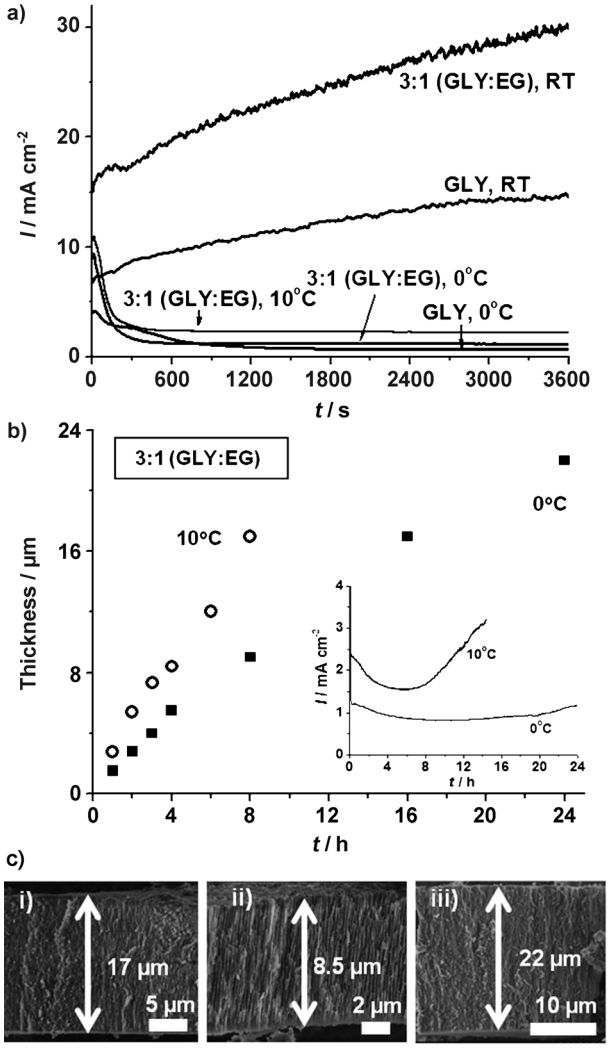

Figure 2. a) Typical anodizing current–time behavior for different electrolytes at different temperatures. Shown are glycerol (GLY) and a mixture of GLY and ethylene glycol (EG), 3:1 (3 M H_2O and 0.54 M NH_4F at 50 V) at room temperature, 10 and 0 °C. b) Thickness of the resulting porous layer as a function of the anodization time that performed at 10 (○) and 0 °C (■). The inset shows the current–time profiles for anodization under the same conditions for periods of 24 and 14 h and for anodization temperature of 0 and 10 °C, respectively. (c) Cross-section view of SEM images of samples anodically grown in the same electrolyte as described in (b) for various designated periods and temperatures at i) 8 h, 10 °C, ii) 8 h, 0 °C, and iii) 24 h, 0 °C.

well-defined nanoporous layers are the current–time profiles as shown in Figure 2a (and as schematically illustrated in Figure 1a ii). In the case of cobalt anodization, a sufficiently high and steady-state current leading to self-organization is only achievable when the anodization is performed at sufficiently low temperature to prevent current self-amplification because of resistive heating (runaway anodization) with continuously increasing currents and an ill-defined mix of O_2 evolution and oxide formation. The effect of temperature control is illustrated in Figure 2 for structures formed at room temperature (RT), 10, and 0 °C. For RT, under any investigated situation runaway oxidation was observed, whereas at 10 and 0 °C in the electrolyte used (a mixed ethylene glycol and glycerol solvent with a volume ratio of 1 to 3, containing 3 M H_2O and 0.54 M NH_4F) ordered structures could be formed. Figure 2b shows a plot for the thickness–time behavior for porous layers grown at 0 and 10 °C. In both cases, the layer thickness grows with time. Nevertheless, after some hours of anodization, dissolution (current increase) is observed and a maximum layer thickness (at 10 °C, about 17 μm) is reached; for prolonged anodization a large portion of the surface is found to peel off as shown in a digital photograph in Figure S5d. At 0 °C, longer anodiza-

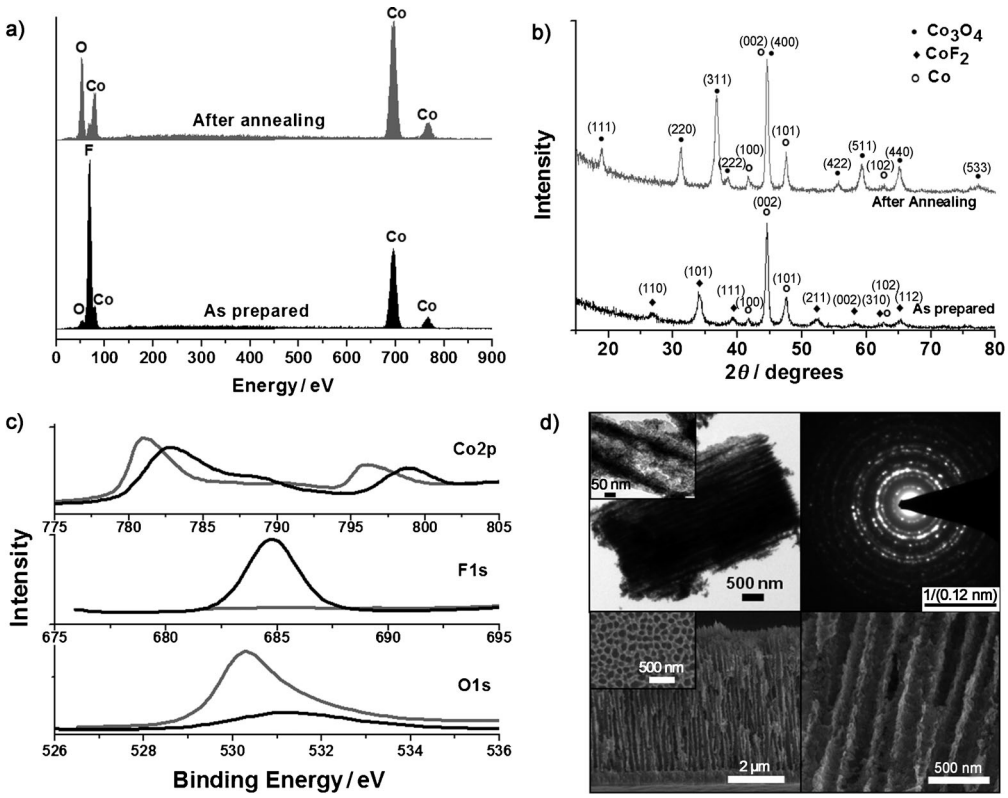

Figure 3. a) EDX spectra and b) XRD patterns of the anodic structure (as prepared and after annealing at 350 °C for 30 minutes). c) Co 2p, F 1s and O 1s XPS spectra of the anodized layer; as prepared (dark curve) and after annealing (gray curve). d) Top left: TEM bright-field image of the structure after annealing to Co_3O_4 at low and high (inset) magnification. Top right: the corresponding selective area electron diffraction pattern. Bottom left: The cross and top (inset) section view SEM images of the annealed Co_3O_4 sample. Bottom right: High-magnification SEM image of the aligned channel geometry in the annealed Co_3O_4 sample.

tion can be performed but the maximum layer thickness is about 22 μm. Figure 2c shows some of the examples for the cross-sections for anodization performed for different durations at 0 or 10 °C.

To gain information on the composition and crystal structure, energy-dispersive X-ray spectroscopy (EDX), XRD, and X-ray photoelectron spectroscopy (XPS) of the as-formed (as-anodized) and annealed layers were acquired. From the EDX spectra in Figure 3a, it is evident that the as-formed layer mainly consists of cobalt fluoride (CoF_2) with about 5 atm% O (this resembles the case of self-organizing anodization of vanadium).[10g] This finding is also in line with XRD analysis (see Figure 3b) where peaks corresponding to crystalline CoF_2 can be identified. Upon a heat-treatment for 30 minutes at 350 °C in air, the layer can be entirely converted to Co_3O_4 (black color, digital photograph of Figure S5e) with the nanoporous structure well maintained (see Figure 4d). This implies that a simple and straightforward heat-treatment approach is sufficient to produce an ordered nanoporous Co_3O_4 surface. From XPS measurements, the Co2p XPS spectra of the annealed sample presented in Figure 3c show two major peaks with binding energy (BE) values at 795.6 and 780.2 eV, corresponding to the $Co2p_{1/2}$ and $Co2p_{3/2}$ spin–orbit peaks, respectively, of the Co_3O_4 phase.[14] The O1s XPS spectra peak with a BE of approximately 530 eV for the annealed sample corresponds to oxygen species in the spinel Co_3O_4 phase.[15] The smaller peak observed close to 532 eV for the as-prepared sample in the O1s spectra indicates possibly the binding with fluoride in the form of O–F that may reflect the amorphous part of the sample. Fluorine is only present in the sample before annealing with a binding energy around 685.54 eV. EDX spectra further confirm the loss of fluorides after the annealing step.

Additionally, Figure 3d shows TEM and SEM images of the Co_3O_4 obtained after the as-anodized nanoporous layer was heat-treated in air at 350 °C for 30 minutes. The nanoporous structure can be readily seen from the top-left TEM image. The inserted higher magnification image shows the thickness of the wall to be approximately 50 to 70 nm. The nanoporous wall consists of crystals with an average size of around 20 nm, and a high degree of crystallinity as evident from the selected-area electron diffraction (SAED) pattern (top right). The diffraction patterns can be entirely indexed with the spinel cubic Co_3O_4 phase. The cross-section SEM image shows the bottom of the annealed nanoporous layer consisting of about 0.3 μm thick compact oxide resulting from thermal oxidation of the cobalt foil (see also SEM images in Figure S9). The SEM images also show that the nanoporous structure remains after annealing, and that a higher crystallinity results in a rougher pore wall morphology.

To demonstrate the functional potential of these ordered nanoporous Co_3O_4 structures, electrochemical studies were carried out using cyclic voltammetry. The measurements were performed in 1M KOH solution, where an application of the formed layers as catalyst for the water oxidation can be readily evaluated. We used directly the cobalt nanoporous layers grown on the metallic cobalt foil as an electrode material (i.e. we took advantage of the fact that anodization leads directly to a back-contacted oxide electrode without the need of using a conductive adhesive medium or binders to fabricate a functional porous oxide electrode). This also has the advantage of retaining the vertically aligned geometry of the nanoporous layers. Figure 4a shows that in comparison to a reference compact oxide layer, a 5.5 μm thick ordered

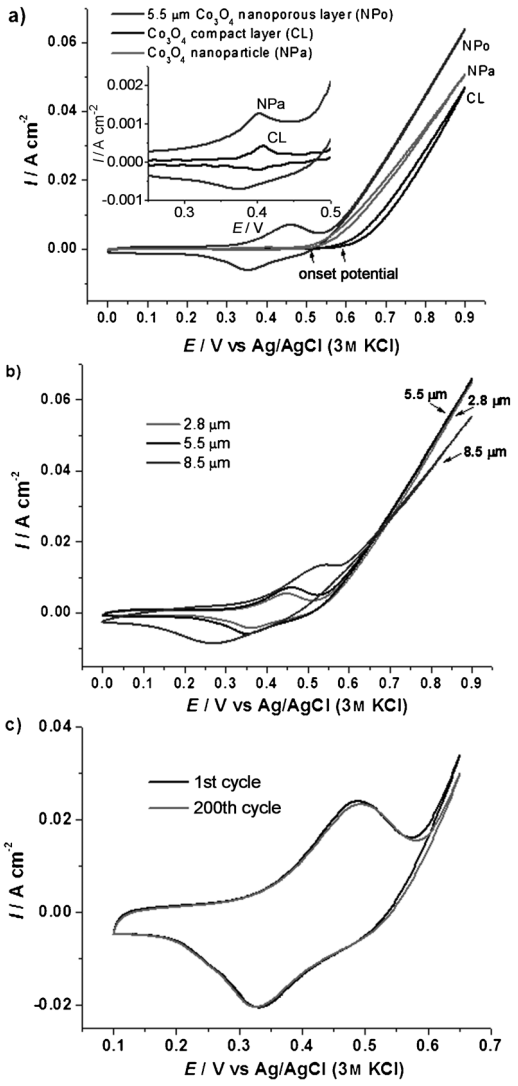

Figure 4. Cyclic voltammograms of different Co_3O_4 layers in 1.0 M KOH with a) comparison to a 5.5 μm thick ordered porous layer on a substrate (obtained by anodization of cobalt in mixed GLY and EG (3:1), 3 M H_2O and 0.54 M NH_4F, at 50 V, 0 °C for 4 h and subsequent annealing) with compact anodic oxide layer and Co_3O_4 (nafion immobilized). b) Comparison of cyclic voltammograms of the nanoporous layers with different thicknesses. c) The stability test showing cyclic voltammograms for the first and 200th cycle. The scan rates employed are for a) and b) 25 mV s^{-1} and for c) 50 mV s^{-1}.

porous Co_3O_4 layer shows a significant lowering of the onset potential required for water oxidation by approximately 100 mV. The advantages of the larger surface area can be seen from the comparison shown in the inset of Figure 4a where drastically increased redox peak currents corresponding to the oxidation of Co^{III} to Co^{IV} are obtained for the porous layer.[16,17] We confirmed through gas chromatography and mass spectroscopy measurements the obtained gas at the anodic compartment to be O_2. To compare the performance of the nanoporous layer to the typical nanoparticle approach, commercially available Co_3O_4 nanoparticles were immobilized on cobalt foil by nafion. In this case, an onset potential of the catalytic reaction comparable with the nanoporous layer is observed. Nevertheless, the nafion immobilized particles yield a significantly lower catalytic current. The redox process from cyclic voltammograms (inset in Figure 4a), indicates that the amount of electroactive Co_3O_4 is much lower for the particle layer, but even for higher Co_3O_4 particle loading no higher catalytic currents could be obtained (see Figure S11). The clearly better performance of the aligned nanoporous layers may be due to the advantageous geometry that allows an optimized use of the electroactive area with minimal ohmic resistance issues (as is the case encountered when using binders) and/or the considerably smaller crystallite size of Co_3O_4 in the nanoporous structure (about 20 nm vs. 50 nm).

As presented in Figure 4b, we further explored the thickness dependence of the obtained nanoporous Co_3O_4 layer towards the electrocatalytic water oxidation performance. Only an insignificant difference in the catalytic currents between the samples of 2.8 and 5.5 μm thicknesses were observed, whereas for 8.5 μm thick layers, a lower catalytic current at potentials above 0.70 V is obtained. From the anodic and cathodic peak positions, a larger peak-to-peak separation is observed, indicating a slower electron-transfer process for the sample with a thicker nanoporous layer. This behavior is characteristic of quasi-reversible diffusion-controlled electron-transfer process (see the scan rate dependence study in Figure S12). From Figure 4b,c, we see that another potential application of nanoporous Co_3O_4 is in redox-based pseudo-capacitors, because a significant enhancement of the capacitance values with the increase of the layer thicknesses is achieved (see enlarged redox peaks in Figure S13). Morever, in the alkaline environment the porous Co_3O_4 layers show excellent stability over 200 cycles (Figure 4c).

In summary, we report for the first time the formation of highly ordered cobalt oxide nanoporous layers using self-organizing electrochemical anodization. This also represents another example (except for iron)[11] for self-organizing anodization of non-valve metals. We demonstrate that by thoroughly optimized electrochemical conditions, competing oxygen evolution can be sufficiently suppressed to reach an anodic formation of the desired nanoporous structures. In the present case a layer rich in fluorides is formed that upon suitable heat-treatment can be readily converted to Co_3O_4. We illustrate that the formed oxide layers have a significant potential for applications such as a catalyst-electrode for water oxidation (towards substitution of conventional catalyst such as IrO_2 or RuO_2),[18] and a pseudo-capacitive material for supercapacitors.

Received: November 1, 2012
Published online: January 9, 2013

Keywords: anodization · cobalt · electrochemistry · nanoporous materials · self-organization

[1] a) M. Valden, X. Lai, D. W. Goodman, *Science* **1998**, *281*, 1647; b) A. T. Bell, *Science* **2003**, *299*, 1688.
[2] a) M. S. Whittingham, *Chem. Rev.* **2004**, *104*, 4271; b) V. Artero, M. Chavarot-Kerlidou, M. Fontecave, *Angew. Chem.* **2011**, *123*,

7376; *Angew. Chem. Int. Ed.* **2011**, *50*, 7238; c) X. Xie, W. Shen, *Nanoscale* **2009**, *1*, 50.
[3] a) M. W. Kanan, D. G. Nocera, *Science* **2008**, *321*, 1072; b) Y. Surendranath, M. Dincă, D. G. Nocera, *J. Am. Chem. Soc.* **2009**, *131*, 2615; c) D. A. Lutterman, Y. Surendranath, D. G. Nocera, *J. Am. Chem. Soc.* **2009**, *131*, 3838; d) M. W. Kanan, Y. Surendranath, D. G. Nocera, *Chem. Soc. Rev.* **2009**, *38*, 109.
[4] W.-Y. Li, L.-N. Xu, J. Chen, *Adv. Funct. Mater.* **2005**, *15*, 851.
[5] a) F. Jiao, K. M. Shaju, P. G. Bruce, *Angew. Chem.* **2005**, *117*, 6708; *Angew. Chem. Int. Ed.* **2005**, *44*, 6550; b) E. L. Salabas, A. Rumplecker, F. Kleitz, F. Radu, F. Schüth, *Nano Lett.* **2006**, *6*, 2977.
[6] K. T. Nam, D. W. Kim, P. J. Yoo, C. Y. Chiang, N. Meethong, P. T. Hammond, Y. M. Chiang, A. M. Belcher, *Science* **2006**, *312*, 885.
[7] a) Z. G. Guo, W. M. Liu, *Appl. Phys. Lett.* **2007**, *90*, 193108; b) L. H. Hu, Q. Peng, Y. D. Li, *J. Am. Chem. Soc.* **2008**, *130*, 16136; c) L. Zhuo, J. Ge, L. Cao, B. Tang, *Cryst. Growth Des.* **2009**, *9*, 1.
[8] H. Masuda, K. Fukuda, *Science* **1995**, *268*, 1466.
[9] V. Zwilling, E. Darque-Ceretti, A. Boutry-Forveille, D. David, M. Y. Perrin, M. Aucouturier, *Surf. Interface Anal.* **1999**, *27*, 629.
[10] a) J. M. Macak, H. Tsuchiya, L. Taveira, S. Aldabergerova, P. Schmuki, *Angew. Chem.* **2005**, *117*, 7629; *Angew. Chem. Int. Ed.* **2005**, *44*, 7463; b) J. Park, S. Bauer, K. Von der Mark, P. Schmuki, *Nano Lett.* **2007**, *7*, 1686; c) S. P. Albu, D. Kim, P. Schmuki, *Angew. Chem.* **2008**, *120*, 1942; *Angew. Chem. Int. Ed.* **2008**, *47*, 1916; d) D. Kim, A. Ghicov, S. P. Albu, P. Schmuki, *J. Am. Chem. Soc.* **2008**, *130*, 16454; e) K. Lee, D. Kim, P. Roy, I. Paramasivam, B. I. Birajdar, E. Spiecker, P. Schmuki, *J. Am. Chem. Soc.* **2010**, *132*, 1478; f) P. Roy, S. Berger, P. Schmuki, *Angew. Chem.* **2011**, *123*, 2956; *Angew. Chem. Int. Ed.* **2011**, *50*, 2904; g) Y. Yang, S. P. Albu, D. Kim, P. Schmuki, *Angew. Chem.* **2011**, *123*, 9237; *Angew. Chem. Int. Ed.* **2011**, *50*, 9071.
[11] a) S. P. Albu, A. Ghicov, P. Schmuki, *Phys. Status Solidi RRL* **2009**, *3*, 64 – 66; b) S. K. Mohapatra, S. E. John, S. Banerjee, M. Misra, *Chem. Mater.* **2009**, *21*, 3048; c) R. R. Rangaraju, A. Panday, K. S. Raja, M. Misra, *J. Phys. D* **2009**, *42*, 135303; d) T. J. LaTempa, X. Feng, M. Paulose, C. A. Grimes, *J. Phys. Chem. C* **2009**, *113*, 16293.
[12] a) P. Skeldon, G. E. Thompson, S. J. Garcia-Vergara, L. Iglesias-Rubianes, C. E. Blanco-Pinzon, *Electrochem. Solid-State Lett.* **2006**, *9*, B47; b) V. P. Parkhutik, V. I. Shershulsky, *J. Phys. D* **1992**, *25*, 1258; c) K. R. Hebert, S. P. Albu, I. Paramasivam, P. Schmuki, *Nat. Mater.* **2012**, *11*, 162.
[13] J. B. Gerken, J. G. McAlpin, J. Y. C. Chen, M. L. Rigsby, W. H. Casey, R. D. Britt, S. S. Stahl, *J. Am. Chem. Soc.* **2011**, *133*, 14431.
[14] a) C. V. Schenck, J. G. Dillard, J. W. Murray, *J. Colloid Interface Sci.* **1983**, *95*, 398; b) M. Oku, Y. Sato, *Appl. Surf. Sci.* **1992**, *55*, 37.
[15] L. Armelao, D. Barreca, S. Gross, E. Tondello, *Surf. Sci. Spectra* **2001**, *8*, 14.
[16] F. Svegl, B. Orel, I. Grabec-Svegl, V. Kaucic, *Electrochim. Acta* **2000**, *45*, 4359.
[17] B. Y. Kim, I.-B. Shim, Z. O. Araci, S. S. Saavedra, O. L. A. Monti, N. R. Armstrong, R. Sahoo, D. N. Srivastava, J. Pyun, *J. Am. Chem. Soc.* **2010**, *132*, 3234.
[18] S. Trasatti, *J. Electroanal. Chem.* **1980**, *111*, 125.

